Astrophysical Masers:
Unlocking the Mysteries of the Universe
Proceedings IAU Symposium No. 336, 2017
A. Tarchi, M.J. Reid & P. Castangia, eds.

doi:10.1017/S1743921317009309

A detailed study toward the Water fountain IRAS 15445-5449

Andrés F. Pérez-Sánchez[1], Rebeca García López[2], Wouter Vlemmings[3] and Daniel Tafoya[3]

[1]European Souther Observatory, Alonso de Córdova 3107, Vitacura, Casilla 19001, Santiago de Chile email: aperezsa@eso.org
[2]Dublin Institute for Advance Studies, 31 Fitzwilliam Place, Dublin 2, Ireland
[3] Department of Space, Earth and Environment, Chalmers University of technology, Onsala Space Obsevatory, 439 92 Onsala, Sweden.

Abstract. Post-Asymptotic giant branch (post-ABG) sources with high-velocity spectral features of H_2O maser emission detected toward their circumstellar envelopes (CSEs) are known as Water Fountain (WF) nebulae. These are low- or intermediate-mass Galactic stellar sources that are undergoing the late stages of an intense mass-loss process. The velocity and the spatial distribution of the H_2O maser spectral features can provide information about the kinematics of the molecular gas component of their CSEs. Hence, observational studies toward WF nebulae could help to better understand the formation of the asymmetric structures (hundred to thousand AUs) commonly seen toward Planetary nebulae (PNe). Here we present preliminary results of observations done toward the WF IRAS 15445-5449 using the Australia Telescope Compact Array (ATCA) and the Very Large Telescope (SINFONI/VLT). Assuming that the pumping of the H_2O maser transitions is a consequence of shocks between different velocity winds, the spatial distribution of the emission shed light on the scales of the regions affected by the propagation of the shock-fronts.

Keywords. stars: AGB and Post-AGB, Masers, stars: late-type.

1. Introduction

The WF nebulae IRAS 15445-5449 was classified as a post-AGB given its position in the MSX color-color diagram (Deacon *et al.* (2007)). Detection of 1612 MHz line was reported by Sevenster *et al.* (1997). Main line observations (1665 MHz and 1667 MHz) were carried out in 1998 (Deacon *et al.* (2007); and references therein). The profile of the spectra detected in all the lines observed (1612 MHz, 1665 MHz, 1667MHz) were classified as irregular, given their broad line profiles (Δv$\geqslant$80km s^{-1}). Although none of the OH line profiles are double-peak, the central velocity of the OH lines was assumed as the systemic velocity of the source (v$_{sys}$ = $-$150 km s^{-1}). Moreover, Deacon *et al.* (2007) reported the detection of high-velocity H_2O maser emission at 22 GHz. The H_2O spectral features were found to be red-shifted with respect to the OH maser lines. Therefore the emission was thought to arise from a red-shifted jet-like structure. Bains *et al.* (2009) reported the detection of radio continuum emission at centimeter wavelengths with negative spectral index ($\alpha < -0.1$) in the frequency range from 4.8 GHz to 8.6 GHz. This result confirmed the negative spectral index retrieved from radio continuum observations carried out between 1998/1999 at 2 GHz, 5 GHz, and 10 GHz (Deacon *et al.* (2007)). The synchrotron jet was confirmed by observations of a spatially resolved radio continuum emission at 22 GHz (Pérez-Sánchez *et al.* (2013)). The detection of a strong non-thermal component in the radio continuum implies a strong magnetic field interacting with relativistic particles. The distribution of the emission, elongated in the north-south direction,

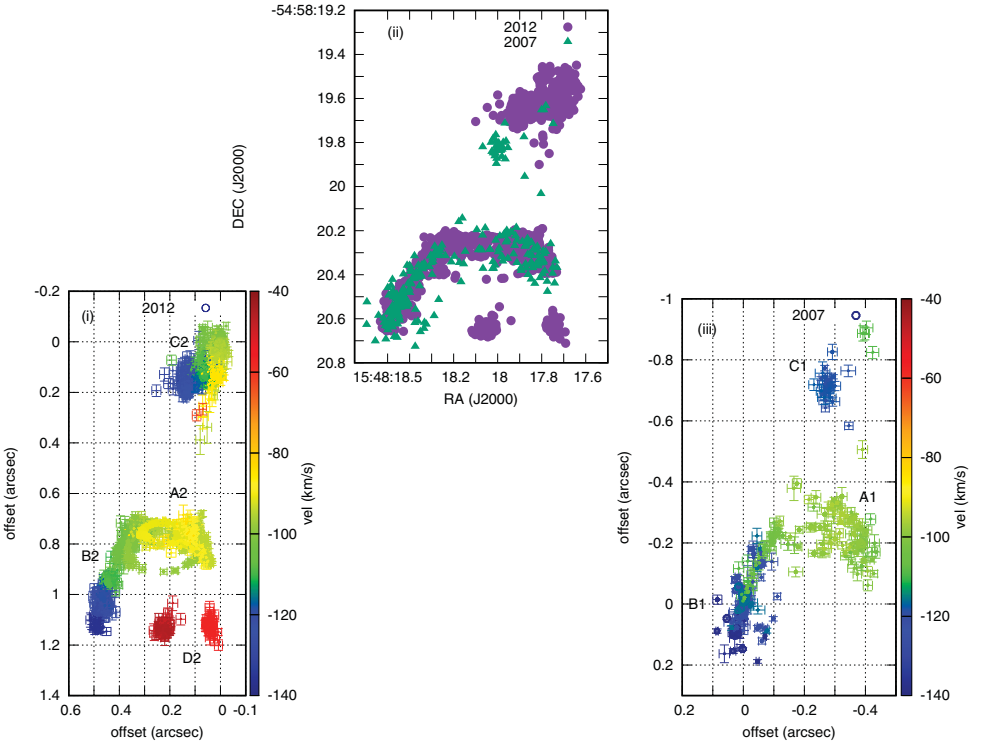

Figure 1. Spatial distribution of the 22 GHz H_2O maser spectral features detected in 2012 (panel i), 2007 (panel iii), and both data sets overlied using the emission in regions B1 and B2 for alignment (panel ii). In panels (i) and (iii) the offsets are with respect to the position of the brightest spectral feature detected in each data set, and the color bar indicates the velocity of the spectral features with respect to $v_{sys} = -96.0$ km s^{-1}. In panel (i) the strongest spectral feature is detected toward region C2, while in the panel (iii) the strongest feature arises from region B1. Panel (ii) shows that the spatial distribution is consistent between the 2012 and 2007 data sets.

is consistent with the hourglass morphology seen in the mid-IR (Lagadec *et al.* 2011). Radio continuum emission, OH and H_2O maser emission; atomic and molecular Hydrogen lines, and CO overtone emission are direct evidence of the energetic activity taking place in large spatial scales within the CSE of the WF IRAS 15445−5449 (Pérez-Sánchez *et al.* in prep).

2. Observations and results

The observing programs were carried out with ATCA in 2007 and 2012, using, respectively, the 6B and 6A array configurations. In both cases the amplitud (1934-638) and phase (1613-586) calibrators observed were the same. The calibration and the imaging of the data was done using MIRIAD (Sault *et al.* 1995). The synthesized beam are $\theta_{2007} = 0.46$"$\times 0.34$" and $\theta_{2012} = 0.5$"$\times 0.35$". The rms in line free channels are $\mathrm{rms}_{2007} \approx 50$ mJy beam^{-1} and $\mathrm{rms}_{2012} \approx 30$ mJy beam^{-1}. The AIPS task SAD was used to fit 2-D gaussian components to the emission above 3-σ within each spectral channel (component fitting). The spectral channel with the strongest peak flux in each spectrum was self-calibrated. With this, the position offset retrieved from each spectral channel is relative to the position of the brightest spectral feature. Pérez-Sánchez *et al.* (2011)

https://doi.org/10.1017/S1743921317009309 Published online by Cambridge University Press

reported 11.8 Jy beam^{-1} as the brightest spectral feature in the 2007 spectrum. From the new component fitting results, to retrieve the position of the different spectral features allowed us to measure the flux of the blended spectral features within the strongest feature reported in 2011. Hence, the brightest of the blended features has peak flux of 6.8±0.2 Jy beam^{-1} at -119.8 km s^{-1}, and arises toward region B1 (Fig. 1). In the 2012 data set, the brightest spectral feature has a peak flux of 6.9±0.07 Jy beam^{-1} and was detected toward region C2 at −98 km s^{-1}. SINFONI/VLT observations yielded spatially resolved emission of shock-excited ro-vibrational transitions of molecular hydrogen (H_2) (Pérez-Sánchez *et al.* in prep). The brigthest spectral feature in the SINFONI data cube is the H_2 1-0 S(1) line (Fig. 2). Its peak wavelength (λ_{peak}) was determined in each pixel along the λ axis of those pixels with emission over 3-σ. The mean peak wavelength ($\bar{\lambda}_{peak}$ = 2.1211 μm) was estimated in order to calculate the Doppler shifting with respect to the rest wavelength of the transition (λ_{rest}=2.1218μm). The resolution unit of the SINFONI cube is 2.45×10^{-4} μm. With this we calculated the systemic velocity v_{sys} = −96.4±34 km s^{-1}. Despite the large error, we estimated the kinematic distances to the source using the velocity retrieved from the H_2 line. Hence, using the kinematic distance calculator (Reid *et al.* 2014) near and far distances are 5.4 ± 0.4 kpc and 8.5 ± 0.4 kpc, respectively.

3. Discussion and conclusions

With the systemic velocity calculated, the interpretation of the velocity and spatial distribution of the H_2O spectral features needs to be revisited. The spatial distribution of the spectral features detected in 2007 displays three different regions in emission (A1, B1, and C1, panel (iii) in Fig. 1). The high-velocity spectral features are found over the same velocity range toward regions B1 and C1. The spectral features in the velocity range from −100 km s^{-1} to −96 km s^{-1} are detected toward the elongated region A1. With respect to v_{sys} = −96 km s^{-1}, the 2007 data set displays only blue-shifted spectral features †. The velocity and spatial distribution of the emission detected in 2012 is consistent with the 2007 distribution. The regions B2 and C2 contains the high-velocity spectral features, again, with features over the same velocity range. All the red-shifted features are detected towards region D2, which has the largest positional offset with respect to B2, A2 and C2. The spectral features within the velocity range from −100 km s^{-1} to −87 km s^{-1} arise from region A2, an elongated structure with similar shape to that of A1. In Fig 1 (panel ii), both data sets were overlied for ilustration. The emission in regions B1 and B2 have similar angular extension and velocity distribution. Most likely the foreground pumped gas moves along the line of sight toward the observer. In this case, the masers in regions B trace a molecular wind with a larger velocity component along the radial direction of a cylindrical reference frame.

The offset between the centroids of regions C1 and C2 is larger than 0.1 arcsec in Dec and ≈ 0.15 arcsec in RA. Such offset could suggest a precessing collimated wind propagating throughout the ionized cavity and colliding the dense internal wall of the hourglass morphology at different heights. Another possible scenario could involve episodic ejections propagating as high-velocity shock-fronts throughout the ionize cavity, which eventually collide with the internal walls of the hourglass structure. In either case, the maser spectral features indicates the large activity and interaction between the ionized cavity and the molecular layers that surrounds it. Hollenbach *et al.* (2013) have shown

† Because the spectral setup, the red-shifted spectral features were not detected in 2007 observations.

https://doi.org/10.1017/S1743921317009309 Published online by Cambridge University Press

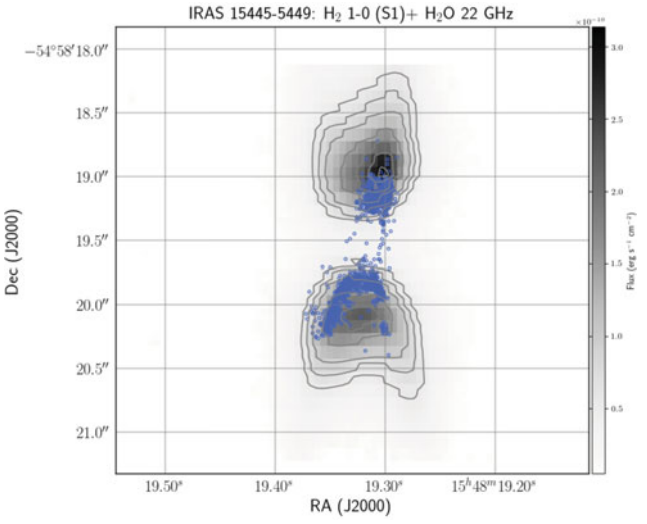

Figure 2. Spatial distribution of the H_2O maser emission (2012, dots) overlaid on the spatial distribution of the H_2 1-0 S(1) ro-vibrational line detected with SINFONI/VLT (gray scale and contours, Pérez-Sánchez *et al.* in prep). The position of the maser features were shifted 0.08 arcsec in RA and 0.4 arcsec in Dec. Assuming that the error in the position of the SINFONI data is ≈1 arcsec, the spatial distribution suggest a strong correlation between the H_2 peaks and the position of the regions with maser emission, therefore supporting a scenario where the maser emission trace postshocks regions of J-type shocks (Hollenbach *et al.* (2013)).

that 22 GHz H_2O maser emission can be generated in the postshock region of J-type shocks ($v_s > 30$ km s^{-1}). The precense of dust grains in the postshock region is key. Molecular hydrogen (H_2) re-forms onto grains surface, and then are ejected to the gas phase. In high postshock densities (n>10^6cm^{-3}) the H_2 ro-vibrational levels are collisionally de-excited. This process mantain the postshock gas temperature in the range 300 K - 400 K, which favor the formation of H_2O. A number of H_2O IR transitions involved in the pumping scheme of the $J_{k_a K_c} = 6_{16}$-5_{23} H_2O upper level are involved in the cooling of the postshock region, leading to an effective inversion of the level population of the 22 GHz H_2O transition. In the case of the WF IRAS 15445-5449, we might be looking at the emission arising from the postshock regions at the foreground molecular layers. Within the error of SINFONI/VLT, the offset between the peak flux of the H_2 ro-vibrational line, and the offsets between regions C, A and B in each data set can be correlated (Fig. 2). This suggest that the emission is being generated in the postshock region following the reformation of H_2 as described by Hollenbach *et al.* (2013).

References

Bains, I., Cohen, M. *et al.* 2009, *MNRAS*, 397, 1386
Deacon, R. M., Chapman, J. M., Green, A. J., & Sevenster, M. N. 2007, *ApJ*, 658, 1096
Hollenbach, D., Elitzur, M., & McKee, C. F. 2013, *ApJ*, 773, 70
Lagadec, E., Verhoelst, T., Mékarnia, D., *et al.* 2011, *MNRAS*, 417, 32
Pérez-Sánchez, A. F., *et al.* 2013, *MNRAS*, 436, L79
Pérez-Sánchez, A. F., Vlemmings, W. H. T., & Chapman, J. M. 2011, *MNRAS*, 418, 1402
Reid, M. J., Menten, K. M., Brunthaler, A., *et al.* 2014, *ApJ*, 783, 130
Sault, R. J. *et al.* 1995, *Astronomical Data Analysis Software and Systems IV*, 77, 433
Sevenster, M. N., Chapman, J. M., Lindqvist, M. *et al.* 1997, *A&AS*, 124, 509

https://doi.org/10.1017/S1743921317009309 Published online by Cambridge University Press